

# Fast T1/B1 Mapping using multiple dual TR RF-spoiled Steady-State Gradient-Echo Sequences

T. Voigt<sup>1</sup>, S. Remmele<sup>2</sup>, U. Katscher<sup>2</sup>, and O. Doessel<sup>1</sup>

<sup>1</sup>Institute of Biomedical Engineering, University of Karlsruhe, Karlsruhe, Germany, <sup>2</sup>Philips Research Europe, Hamburg, Germany

**Introduction:** Dynamic Contrast-Enhanced MRI (DCE-MRI) is widely applied to assess tissue perfusion and vascular permeability [1]. In most of these applications, a  $T_1$  map, obtained prior to contrast agent (CA) administration, is used to convert the signal intensity from a series of  $T_1$ -weighted spoiled gradient-echo images into CA concentration. The accuracy of the approach is mainly affected by the flip angle dependency of the steady-state signal, which necessitates careful quantification of  $B_1$  inhomogeneities in advance [2]. This study investigates a new approach called “Multiple TR  $B_1/T_1$  Mapping” (MTM), capable of fast, simultaneous  $B_1$  and  $T_1$  mapping [3]. This approach is based on the “Actual Flip angle Imaging” (AFI) sequence [4], but uses multiple TR pairs instead of the standard AFI approach of a single TR pair. Recently, MTM has been investigated in terms of  $B_1$  mapping performance [3]. In this work, MTM is analysed with respect to its  $T_1$  mapping performance in comparison with an inversion recovery reference sequence and in due consideration of the limited time allowed in a clinical set-up.

**Theory:** The standard AFI employs a dual TR RF-spoiled steady-state gradient-echo sequence. The signal intensities  $S_1$  and  $S_2$  measured in the intervals  $TR_1$  and  $TR_2$ , can be described analytically [4] (Eq. 1). The coefficient  $F_i$  is different for signals  $S_1$  and  $S_2$ . For the first image  $S_1$ , it is

$$S(TR_1, TR_2, TE, T_2^*, T_1, \alpha, \tilde{M}_0) = M_0(T_2^*, TE, \tilde{M}_0) \cdot F_i(TR_1, TR_2, \alpha, T_1) \quad (1)$$

$$F_i(\alpha, T_1) = ((1 - E_2) \sin \alpha + \frac{1}{2}(1 - E_1)E_2 \sin 2\alpha) / (1 - E_1 E_2 \cos^2 \alpha) \quad (2)$$

given in Eq. (2), with  $M_0 = \tilde{M}_0 \cdot e^{-TE/T_2^*}$  and  $E_{1,2} = e^{-TR_{1,2}/T_1}$ .  $S_2$  can be obtained from Eq. (2) by interchanging indices. MTM employs multiple dual TR sequences using different  $TR_1$ ,  $TR_2$  in subsequent measurements. Each dual TR sequence yields two data points  $F_1(TR_1, TR_2, \alpha, T_1)$  and  $F_2(TR_2, TR_1, \alpha, T_1)$  from signals  $S_1$  and  $S_2$  for each pixel. The parameters  $\alpha$ ,  $T_1$ , and  $M_0$  can then be obtained by a numerical fit of the theoretical expressions for the signal intensities Eqs. (1,2) to the set of measured data points. Hereby,  $\alpha$  and  $T_1$  are obtained simultaneously and independently of each other. Thus, no further correction of either parameter has to be made, and no systematic  $B_1/T_1$  errors are present in this method. Sequence parameters can be optimized to allow for optimal  $B_1$  and/or  $T_1$  mapping. In this study, the Cramer Rao Theorem (CRT) [5] was used to achieve best  $T_1$  mapping performance.

**Subjects and methods:** (1) Sequence parameters for MTM were optimized with respect to maximum SNR in  $T_1$  mapping using CRT. For optimization, a target  $T_1 = 900$ ms was chosen. SNR of MTM  $T_1$  mapping was predicted as a function of  $T_1$ . (2) Experiments were conducted using a 1.5T clinical scanner (Philips Healthcare, Best, The Netherlands) on a calibrated phantom (Test Object 5, Eurospin II Test System, Diagnostic Sonar LTD). An in-plane resolution of  $0.98 \times 0.98$  mm<sup>2</sup> and 10mm slice thickness (4 slices) was chosen. MTM  $T_1/B_1$  mapping was applied using  $TR_{11,12} = 115/750$  ms,  $TR_{21,22} = 105/202$  ms, and  $TR_{31,32} = 105/130$  ms. An inversion recovery single shot TSE sequence (IR-TSE) served as an independent  $T_1$  measurement (TR = 10s, IR delays [ms] = 5000, 2244, 1582, 1188, 906, 686, 506, 353, 221, 105). For better comparison, acquisition times were adjusted to approximately 5 min each. (3) The same MTM sequence was tested on a healthy volunteer using the same 1.5T scanner.

**Results/Discussion:** Predicted SNR via CRT and measured SNR for MTM  $T_1$  mapping are shown in Fig. 1. IR-TSE  $T_1$  map is shown in Fig 2a. MTM  $T_1$  and  $B_1$  maps are shown in Fig. 2b and 2c. A quantitative comparison is shown in Fig. 3. MTM  $T_1$  phantom results were found in agreement with manufacturer specifications. The maximum deviation from the true value was 126 ms for MTM and 257 ms for IR-TSE. In comparison with IR-TSE, MTM results were superimposed by stronger noise. Maximum noise (1/SNR) was 11.5% for MTM and 1.4% for IR-TSE. *In vivo* MTM  $T_1$  and  $B_1$  results are shown in Fig. 3.

**Conclusion:** Efficient and accurate baseline  $T_1$  and  $B_1$  quantification is a pre-requisite for standardized and clinical DCE-MRI. This work presents an approach to fast and simultaneous  $T_1$  and  $B_1$  mapping. Fitting of a theoretical model to a steady-state gradient-echo signal delivers independent  $T_1$  and  $B_1$  values. Adjusted in scan time (5min), MTM  $T_1$  mapping was found to be more accurate than IR-TSE in calibrated phantom measurements at the expense of the SNR of the delivered  $T_1$  maps. It is expected that the SNR of MTM can be enhanced by combining MTM with an EPI read out scheme.

**References:** [1] Padhani AR, JMIR 16 (2002), 407-422 [2] Treier R, et al., MRM 57 (2007), 568-576 [3] Voigt T. et al., ISMRM (2009), 4543. [4] Yarnykh VL., MRM 57 (2007), 192-200. [5] Kay SM. Fundamentals of Statistical Signal Processing: Estimation Theory. Englewood Cliffs, NJ: Prentice Hall; 1993.

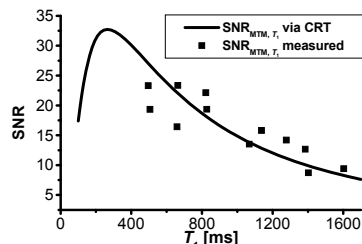


Fig. 1: Predicted and measured SNR of MTM  $T_1$  mapping.

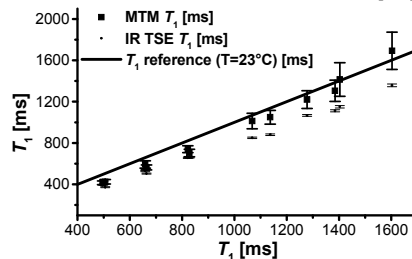


Fig. 3: quantitative comparison of  $T_1$  mapping results from MTM and IR-TSE.

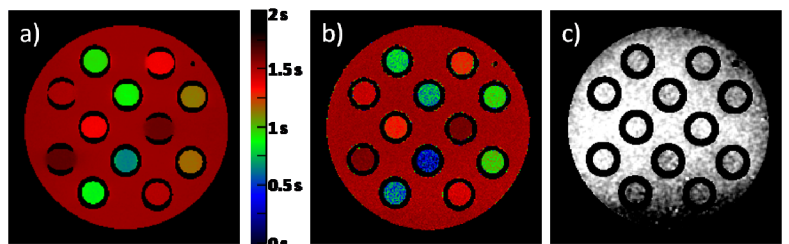


Fig. 2: IR-TSE  $T_1$  map (a) and MTM  $T_1$  map (b). MTM does also provide a  $B_1$  map (c).  $T_1$  values provided by manufacturer (left to right, top to bottom,  $T=23^\circ\text{C}$ , units [ms]): 1278, 822, 664, 1385, 1137, 828, 496, 506, 1603, 1063, 1403, 659.

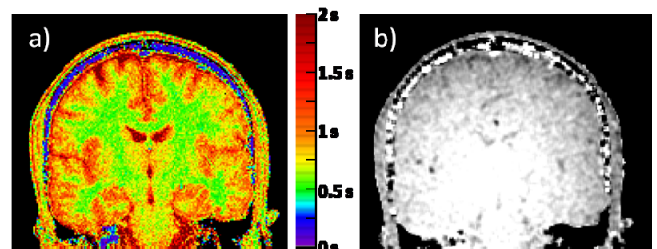


Fig. 4: *In vivo* MTM  $T_1$  map (a) and  $B_1$  map (b).